Self-Assembled Hierarchical MoO_2/Graphene Nanoarchitectures and Their Application as a High-Performance Anode Material for Lithium-Ion Batteries

Yongming Sun, Xianluo Hu,* Wei Luo, and Yunhui Huang*

State Key Laboratory of Material Processing and Die & Mold Technology, School of Materials Science and Engineering, Huazhong University of Science and Technology, Wuhan 430074, P. R. China

ABSTRACT Self-assembled hierarchical MoO_2/graphene nanoarchitectures have been fabricated on a large scale through a facile solution-phase process and subsequent reduction of the Mo-precursor/graphene composite. The as-formed MoO_2/graphene nanohybrid as an anode material for lithium-ion batteries exhibits not only a highly reversible capacity but also an excellent cycling performance as well as good rate capability. Results show that the hierarchical rods made of primary MoO_2 nanocrystals are uniformly encapsulated within the graphene sheets. The synergistic effect of the hierarchical nanoarchitecture and the conducting graphene support may contribute to the enhanced electrochemical performances of the hybrid MoO_2/graphene electrode. This work presents a facile synthetic strategy that is potentially competitive for scaling-up industrial production. Besides, the MoO_2/graphene hybrids with a well-defined hierarchical topology not only provide flexible building blocks for advanced functional devices, but are also ideal candidates for studying their nanoarchitecture-dependent performances in catalytic and electronic applications.

KEYWORDS: nanohybrid · lithium ion battery · self-assembly · hierarchical nanostructures

Lithium-ion batteries, as a major breakthrough in electrochemical energy conversion and storage devices, have been intensively pursued during the past decade. This topic is of key importance for upcoming mobile electric devices and hybrid vehicles because of the high energy density and long cycle lifetime of lithium-ion batteries.[1−3] Currently, a major research direction appears to be shifting to design, fabrication, and manipulation of various lithium-ion battery materials with high reversible capacity, long cycle life, and low cost.[4,5] For instance, transition metal oxides including Fe_2O_3, Fe_3O_4, V_2O_5, and Co_3O_4 are capable of Li^+ insertion/extraction in excess of 6 Li per formula unit. They have attracted a lot of interest recently as anode materials for lithium-ion batteries due to their higher theoretical capacities than that of commercial graphite.[6−9] However, an intrinsically induced drastic volume change gives rise to pulverization that may block the electrical contact pathways in the metal-oxide electrodes, thus leading to a rapid decay in capacity and limiting the potential use.[10] Therefore, developing new synthetic strategies to fabricate high-performance metal-oxide electrode materials with both large reversible capacity and long cycle life still remains a great challenge to chemists and materials scientists.

Nanostructuring of electrode materials can enhance the electrochemical performances that could not be achieved in bulk materials, benefiting from the larger surface area and shorter diffusion path in nanostructured materials.[11] In particular, hierarchically nanostructured inorganic materials have aroused much interest in a variety of fields because of their extraordinarily high active surface/interface and robust stability.[12−18] Electrode materials with a hierarchical nanoarchitecture exhibit intriguing properties by taking advantage of both the nanometer-size effects and the high stability of the secondary-structure assemblies.[12−15] Moreover, carbon coating has been widely used to prevent the exfoliation of active materials and improve the electrical conductivity of electrode materials.[19,20] Nevertheless, the carbon coating often covers the surface of the active materials tightly, and therefore it somehow cannot effectively release the large strain from the volume expansion. Thus, there may be increased resistance for lithium ions to reach the interior active materials. Graphene exhibits superior electrical conductivity, large surface area, structural flexibility, and

* Address correspondence to huxl@mail.hust.edu.cn, huangyh@mail.hust.edu.cn.

Received for review May 17, 2011 and accepted August 8, 2011.

Published online August 08, 2011
10.1021/nn201802c

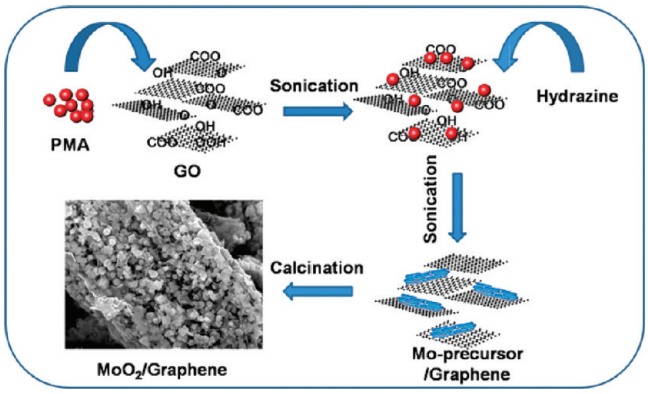

Figure 1. Schematic representation of the fabrication process of the MoO_2/graphene hybrid.

chemical stability. It can host nanostructured electrode materials for energy applications.[21−26] The graphene layers can provide a support for anchoring nanoparticles and work as a highly conductive matrix for good contact between them. Importantly, graphene layers prevent the volume expansion/contraction and the aggregation of nanoparticles effectively during charge and discharge processes.[21−26] Meanwhile, the integration of inorganic nanostructures with the graphene layers may reduce the restacking of graphene sheets and consequently maintain the high surface area. In this regard, both the lithium-storage capacity and the cycling performance of graphene-based nanomaterials will be improved.

Owing to the low electrical resistivity, high stability, and high density (6.5 g cm^{-3}) associated with volume capacity, molybdenum dioxide (MoO_2) has recently received much attention in lithium-ion batteries since its first proposal as a host material 30 years ago.[27] It is reported that nanostructural MoO_2-based materials hold the promise of an enhanced capacity higher than that of their bulk counterparts.[28−33] However, both the long cycle-life (*e.g.*, >50 cycles) and high-capacity (*e.g.*, >500 mAh g^{-1}) MoO_2-based electrode materials have never been reported for lithium storage. Based on the conversion or insertion reactions, the pulverization problem often occurs in the MoO_2-based electrodes during the discharge/charge cycling.[31,34] As a result, the electrical-contact pathways may be blocked and the capacity fades severely. To meet the ever-increasing nanotechnological and energy demand, the diversity of desired nanoarchitectures for high-capacity and long-lifetime MoO_2-based materials still needs to be greatly expanded. Here we report the large-scale fabrication of unprecedented self-assembled hierarchical MoO_2/graphene nanoarchitectures through a facile solution-based method combined with a subsequent reduction process. It is found that the as-formed MoO_2/graphene nanohybrid comprises both the hierarchical MoO_2 nanostructures and the conducting graphene sheets. When used as an anode material, it exhibits highly reversible capacity, excellent cyclic performance, and good rate capability.

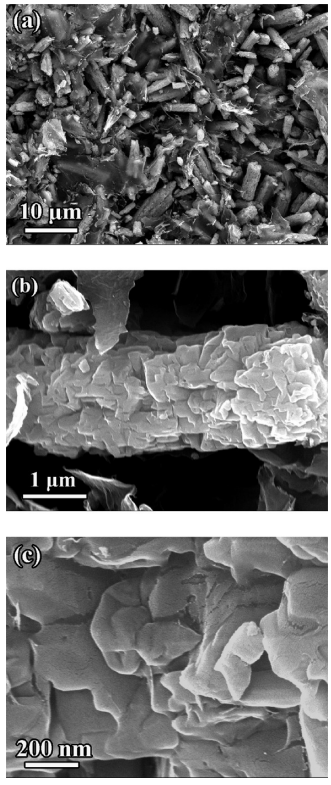

Figure 2. (a−c) SEM images of the Mo-precursor/graphene hybrid.

RESULTS AND DISCUSSION

Figure 1 illustrates the preparation process of the hierarchical MoO_2/graphene nanoarchitectures. Typically, phosphomolybdic acid (PMA) and graphene oxide (GO) reacted with hydrazine hydrate in solution to produce a Mo-precursor/graphene composite. Then, the resulting composite was further annealed at 500 °C for 5 h in a reducing H_2/Ar atmosphere, and self-assembled hierarchical MoO_2/graphene nanoarchitectures were finally formed. The time-dependent experiments for the reactions in solution have been carried out to study the self-assembly process (Figure S1, see Supporting Information). It is proposed that three

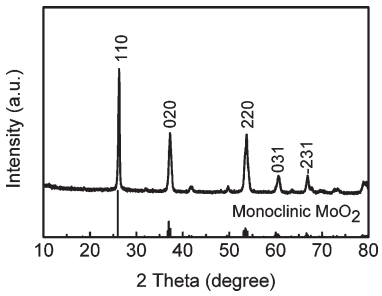

Figure 3. Representative XRD pattern of the resulting MoO_2/graphene hybrid.

main steps are probably included in the formation of the hierarchical MoO_2/graphene hybrids: (a) assembly of graphene and "heteropoly blue" (HPB) clusters, (b) HPB rods wrapped with graphene sheets, and (c) *in situ* formation of graphene-wrapped hierarchical MoO_2 rods in a reducing atmosphere. Moreover, the annealing temperature plays a crucial role in the morphology and the structure of the product. At an annealing temperature of 400 °C or below, the product contains some impurities, instead of monoclinic MoO_2 and graphene. Although the annealing treatment at a higher temperature of 600 °C results in the high crystallinity of the product, MoO_2 particles with larger sizes were formed.

The field-emission scanning electron microscopy (FESEM) images of the Mo-precursor/graphene intermediate are shown in Figures 2a−c. Evidently, the product is composed of many hierarchical rods with diameters of *ca.* 1−3 μm and rough surfaces that are wrapped with graphene nanosheets. Also, some free graphene nanosheets are observed, which connect the hierarchical Mo-based rods. Energy-dispersive X-ray (EDX) microanalysis (Figure S2, see Supporting Information) confirms the existence of Mo, N, O, and C in the Mo-precursor/graphene intermediate. In the control experiments, we also prepared the bare Mo-based precursor without using graphene (Figure S3, see Supporting Information). Similarly, the bare Mo-precursor displays a rod-like shape but a smoother surface (Figure S4, see Supporting Information).

Figure 3 shows the X-ray diffraction (XRD) pattern for the final MoO_2-graphene product prepared by annealing the Mo-precursor/graphene intermediate at 500 °C for 5 h in a 5% H_2/Ar atmosphere. All the diffraction peaks are readily indexed to a pure monoclinic phase [space group: $P2_1/c$ (No. 14)] of MoO_2 (JCPDS No. 65-5787; a = 5.6109 Å, b = 4.8562 Å, c = 5.6285 Å; β = 120.95°). No characteristic peaks were observed for impurities such as phosphates and MoO_3 as well as other molybdenum oxides. After the same thermal treatment, pure monoclinic MoO_2 was also obtained (Figure S5, see Supporting Information). Important information on the surface electronic state and the composition of the final products can be further provided by X-ray photoelectron spectroscopy (XPS). A typical survey XPS spectrum for the MoO_2/graphene product (Figure 4a) involves four distinct peaks at 233.9 (Mo 3d), 398.0 (Mo $3p_{3/2}$), 415.6 (Mo $3p_{1/2}$), and 531.9 (O 1s) eV, characteristic of molybdenum oxides.[35] The Mo 3d peak is further examined by high-resolution XPS (Figure 4b). The Mo $3d_{5/2}$ peak is centered at 229.4 eV, whereas the Mo $3d_{3/2}$ peak is found at 232.5 eV, with a spin energy separation of 3.1 eV. This characteristic doublet of core-level Mo $3d_{5/2,3/2}$ indicates the Mo(IV) oxidation state of MoO_2.[35] In addition, the peaks at 231.8 and 235.3 eV could be ascribed to Mo(VI) $3d_{5/2}$ and $3d_{3/2}$ of MoO_3, respectively, resulting from the slight surface oxidation of metastable MoO_2 in air.[36] The high-resolution C 1s spectrum of the MoO_2/graphene hybrid is shown in Figure 4c. It can be deconvolved into four peaks corresponding to carbon atoms in different oxygen-containing functional groups:[37] (a) nonoxygenated C at 284.5 eV, (b) carbon in C−O at 286.1 eV, (c) carbonyl carbon (C═O, 287.9 eV), and (d) carboxylate carbon (O−C═O, 289.0 eV). The strong C 1s peak (284.5 eV) is related to graphitic carbon in graphene, while the weaker ones from the oxygenated carbons indicate the deoxygenation process accompanying the reduction of graphene oxide. The small O 1s peak at 532.6 eV indicates the presence of residual oxygen-containing groups bonded with C atoms in graphene (Figure 4d).[38]

Figure 5 shows the representative FESEM images for the MoO_2/graphene product. Clearly, no significant change in the morphology was observed in comparison to the Mo-precursor/graphene intermediate. A large number of hierarchical rods like "maize cobs" (~1−3 μm in diameter and *ca.* 5−10 μm in length) exist in the product. At a higher magnification (Figure 5c,d), the hierarchical nanoarchitectures of the MoO_2/graphene composite are clearly observed. Primary MoO_2 nanocrystallites of *ca.* 30−80 nm are wrapped in the graphene layers and assembled into the secondary rods. The corresponding EDX spectrum (Figure S6, see Supporting Information) confirms the presence of Mo, O, and C in the MoO_2/graphene product, which is consistent with the XRD and XPS results (Figures 3 and 4). In comparison, the bare MoO_2 particles obtained from the same experimental condition show a much larger size (Figure S7, see Supporting Information). Furthermore, the elemental distribution of Mo, O, and C in the MoO_2/graphene product was explored (Figure 6), suggesting that the MoO_2 nanoparticles are uniformly wrapped within the graphene sheets. This is beneficial to prevent the MoO_2 nanocrystals from agglomeration, and enables the good dispersion of the MoO_2 particles over the graphene support.

To provide further insights into the morphology and structure on the resulting MoO_2/graphene hierarchical nanostructures, transmission electron microscopy (TEM) investigations were carried out. Figure 7a shows a typical bright-field TEM image at a low magnification for

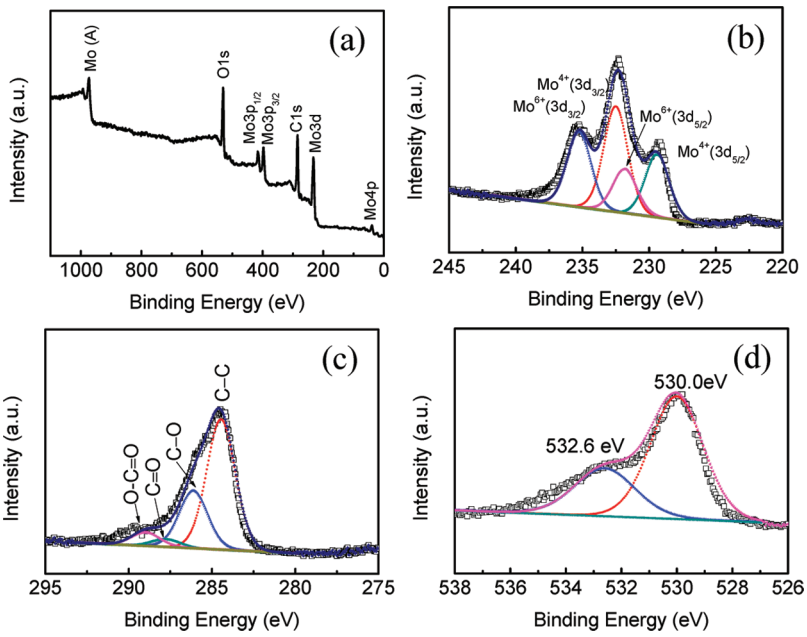

Figure 4. XPS spectra for the MoO_2/graphene hybrid: (a) survey spectrum and high-resolution (b) Mo 3d, (c) C 1s, and (d) O 1s spectra.

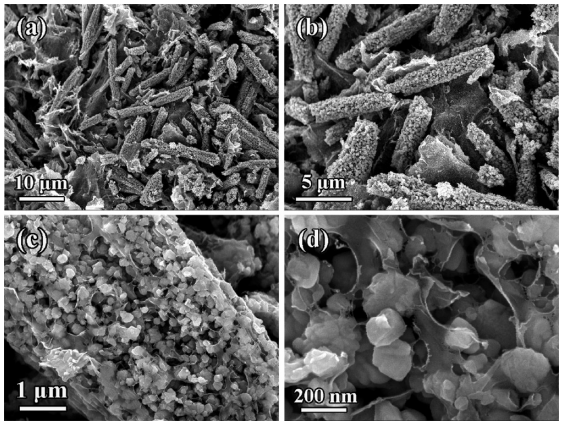

Figure 5. FESEM images of the hierarchical MoO_2/graphene hybrid.

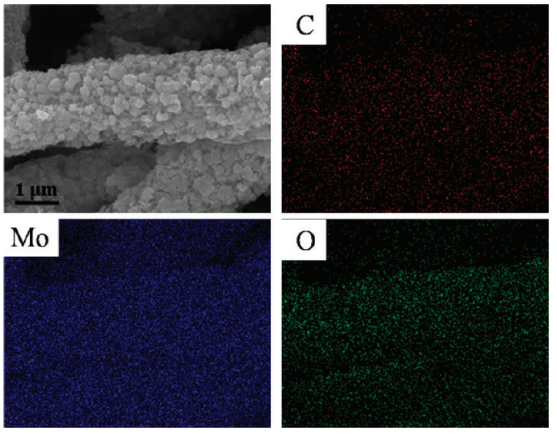

Figure 6. SEM image and the corresponding elemental mapping of C, Mo, and O in the MoO_2/graphene hybrid.

the product. It is clearly observed that the rodlike assemblies comprise numerous primary MoO_2 nanocrystals. The selected-area electron diffraction (SAED) rings reveal that the hierarchical MoO_2 rods are polycrystalline (Figure 7b). The TEM image at a higher magnification (Figure 7c) shows that the MoO_2 crystallites are well wrapped with the graphene nanosheets. Figure 7d shows a high-resolution TEM (HRTEM) image taken from the edge of an individual graphene/MoO_2 assembly. The lattice fringes are clearly observed along the $[\bar{1}13]$ zone axis of MoO_2. The periodic fringe spacings of ~1.7 and ~1.8 Å agree well with the interplanar spacings between the $\{220\}$ and $\{1\bar{2}1\}$ planes of monoclinic MoO_2, respectively. Moreover, a nanolayer of several nanometers exists on the surface of the MoO_2 nanocrystals (Figure 7d). The interplanar spacing of ~0.37 nm corresponds to the separation between (002) lattice planes of graphite. This verifies that the MoO_2 nanocrystal assemblies are well wrapped in the nanocarbon layer of graphene sheets. The significant structural changes during the chemical processing from graphene oxide to graphene are further characterized by Raman spectroscopy (Figure S8, see Supporting Information). Clearly, the characteristic D band at ~1345 cm^{-1} and G band at ~1586 cm^{-1} are observed for the MoO_2/graphene hybrid. The D/G intensity ratio in the MoO_2/graphene hybrid is increased in comparison to that GO, indicating the decreased size of the sp^2 domains after reduction of the graphene oxide.[39] Also, more graphitic domains that have smaller sizes compared with GO may be created during the reduction reaction.

Thermogravimetric (TG) analysis and differential thermal analysis (DTA) of the products were performed in flowing air. Figure 8a shows the TG/DTA result for the as-prepared graphene sheets. Clearly, the weight of graphene is almost lost before 620 °C. The large

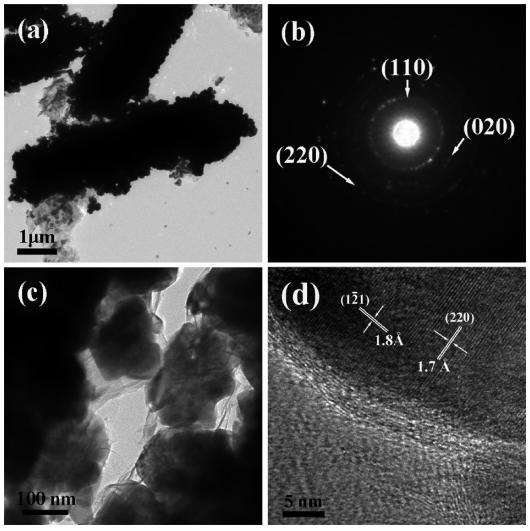

Figure 7. (a) TEM image, (b) SAED pattern, (c) TEM image (higher magnification), and (d) HRTEM image of the MoO_2/graphene product.

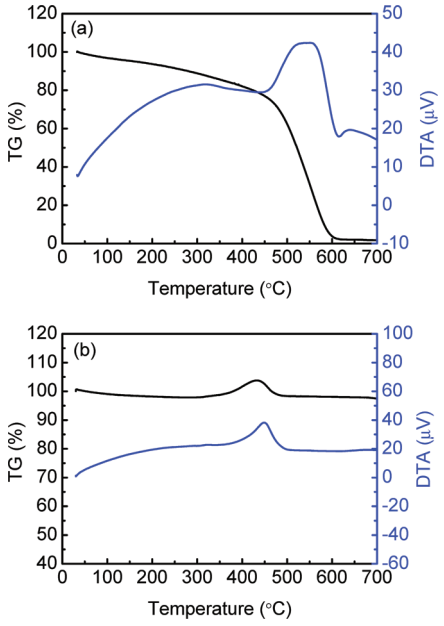

Figure 8. TG and DTA curves of the as-prepared (a) graphene sheets and (b) MoO_2/graphene hybrid.

exothermic peak between 420−620 °C in the DTA profile can be assigned to the combustion of the graphene. Figure 8b shows the TG/DTA result for the as-formed MoO_2/graphene hybrid. The weight change between 200 and 650 °C is due to both the oxidation of MoO_2 and the combustion of graphene. The theoretical value of the weight increase from MoO_2 to MoO_3 is 12.5 wt %; the graphene content in the MoO_2/graphene hybrid is evaluated to be about 11.2 wt %.

The electrochemical properties of the hierarchical MoO_2/graphene product were investigated. Figure 9a shows the cyclic voltammetry (CV) curves of the

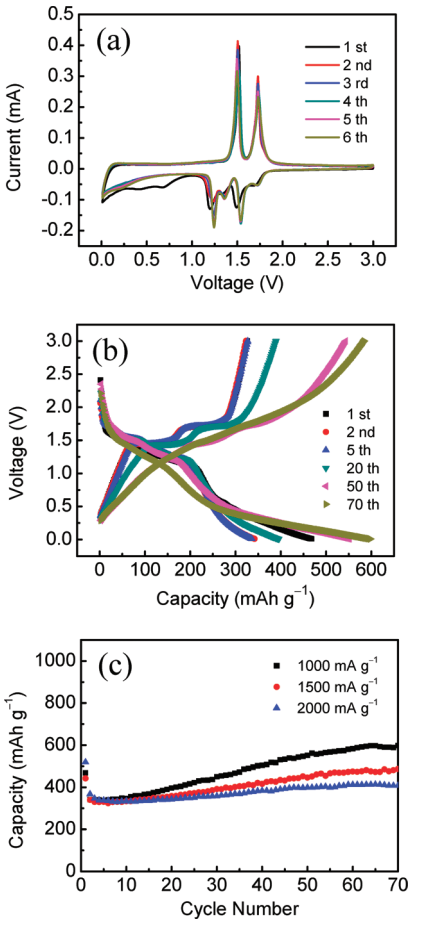

Figure 9. (a) CVs of the MoO_2/graphene hybrid at a scan rate of 0.1 mV s^{-1} in the range of 3−0.01 V *vs* Li. (b) Discharge and charge curves at a current density of 1000 mA g^{-1} in the range of 3−0.01 V *vs* Li. (c) Cycling performance of the MoO_2/graphene composite electrodes in the range of 3−0.01 V *vs* Li at various current densities of 1000, 1500, and 2000 mA g^{-1}.

electrode of the MoO_2/graphene hybrid at a scan rate of 0.1 mV s^{-1} over the range of 0.01−3 V. In the first cycle, two pronounced reduction peaks were observed at 1.49 and 1.20 V, which may arise from a phase transition from the orthorhombic to the monoclinic phase due to the Li insertion.[28,40] An irreversible reduction peak at ~0.7 V corresponds to the irreversible reduction of electrolyte and the formation of a passivating surface film, which disappeared in the following cycles. Two sharp oxidation peaks were observed at 1.50 and 1.73 V, and could be assigned to the phase transitions from the monoclinic to the orthorhombic phase and from the orthorhombic to the monoclinic phase in the Li extraction process, respectively. In the subsequent cycles upon cycling, two evident redox couples at 1.54/1.73 V and 1.24/1.50 V are highly reversible. They correspond to the reversible phase transitions of partially lithiated Li_xMoO_2 during lithium insertion and extraction.[28,40] The second and onward CV curves remain steady, indicating the highly reversible redox reactions of this hybrid. For the bare

MoO_2 electrode (Figure S9, see Supporting Information), two redox peaks locate at 1.54/1.73 V and 1.24/1.50 V in the second cycle, corresponding to the phase transition in the partially lithiated Li_xMoO_2.[40] In the subsequent cycles, however, they decline rapidly, suggesting the poor reversibility. Figure 9b shows the discharge and charge curves for the MoO_2/graphene hybrid at a current density of 1000 mA g^{-1} over the range of 3−0.01 V *vs* Li^+/Li. It is observed that the initial discharge and charge capacities are 468.2 and 342.0 mAh g^{-1}, respectively, and hence an irreversible capacity loss of 27.0%. No obvious potential plateau appears in the first cycle. From the second cycle onward, the capacity of the electrode does not decay, and it reaches 597.9 mAh g^{-1} over 70 cycles with a Coulombic efficiency of ~98%. Two discharge plateaus at about 1.55 and 1.33 V and two charge plateaus at 1.42 and 1.69 V are clearly observed. As suggested by Shi *et al.*[28] and Dahn *et al.*,[40] the inflection point between these plateaus may be ascribed to the phase transitions between the monoclinic and orthorhombic phases in the partially lithiated Li_xMoO_2. These phase transitions are highly reversible in the redox processes, in a good agreement with the CV results. The electrochemical performance of the MoO_2/graphene hybrid is superior to that of the bare MoO_2 anode that loses the capacity severely upon cycling even at much lower current densities (Figure S9, see Supporting Information). In contrast, the electrode made of the MoO_2/graphene hybrid maintains high cyclability, and its reversible capacity even gradually increases. After the second cycle, the Coulombic efficiency of the MoO_2/graphene electrode remains nearly 100% until the 70th cycle at a current density of 1000 mA g^{-1}. Importantly, the MoO_2/graphene electrode, still exhibits an excellent cyclic performance at a much higher current density of 2000 mA g^{-1}, and the capacity reaches 407.7 mAh g^{-1} after 70 discharge and charge cycles (Figure 9c). When tested at a lower current density of 500 mA g^{-1} (data not shown), the capacity is as high as 848.6 mAh g^{-1} after 70 cycles, even higher than the theoretical capacity of both bulk MoO_2 (838 mAh g^{-1}) and graphite (372 mAh g^{-1}).

The electrochemical impedance spectra of the MoO_2/graphene electrode after different discharge/charge cycles over the frequency range from 100 kHz to 0.1 Hz were also measured (Figure 10). The Nyquist plots for the sample after different cycles were similar, displaying a depressed semicircle in the high-middle frequency region and an oblique straight line in the low frequency region. These plots with small semicircle diameters suggest that the MoO_2/graphene hybrid electrodes possess low contact and charge-transfer impedances. There is only a slight increase in semicircle diameters even after 70 discharge and charge cycles, indicating the good stability of the as-prepared electrodes.

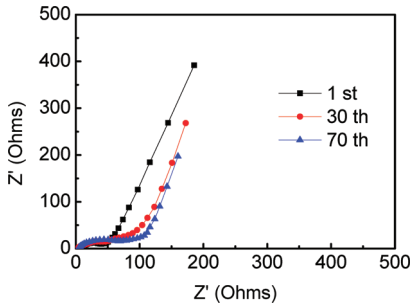

Figure 10. Electrochemical impedance spectra of the MoO_2/graphene electrode after different discharge/charge cycles over the frequency range from 100 kHz to 0.1 Hz.

Compared with previously reported MoO_2 nanostructures,[28−33] the enhanced cycle life and capacity of the MoO_2/graphene electrode may be attributed to the unique hierarchical nanoarchitectures composed of the primary MoO_2 nanocrystals and ultrathin graphene sheets, featuring the high active surface area and the secondary nanostructure. The Barrett−Joyner−Halenda (BJH) analysis shows that the main pore size is about 2.2 nm. The as-prepared MoO_2/graphene hybrid has a specific surface area (BET) of 39.2 m^2 g^{-1} and a pore volume of 0.15 cm^3 g^{-1} (Figure S10, see Supporting Information) by calculations based on the isotherms. The graphene sheets as an elastic buffer may accommodate the volume expansion/contraction during the Li insertion/extraction processes, and thus the cracking or crumbling of the electrode material upon progressive cycling is prevented.[21−26] To confirm the effect of the graphene to buffer the volume effect during the discharge and charge process, the morphology change of the electrode after electrochemical cycling was studied (Figure S11, Supporting Information). It is found that the hierarchical MoO_2/graphene nanoarchitectures can be maintained in the electrodes. When discharged−charged at a current density as high as 2000 mA g^{-1} (Figure S11, Supporting Information), the MoO_2/graphene hybrid still retains its original morphology even after 70 cycles. This further indicates good stability of the hierarchically nanostructured electrodes. Importantly, the hierarchical MoO_2 assemblies are well connected by the conductive graphene sheets with a good electrical conductivity (Figure S12, Supporting Information). This is beneficial to reduce the inner resistance of the lithium-ion batteries and stabilize the electronic and ionic conductivity, therefore leading to a high specific capacity. On the other hand, the Li-ion diffusion is highly dependent on the transport length and accessible sites on the surface of active materials.[11] Owing to the large electrode/electrolyte contact area, short path length for Li^+ transport, and good stability of hierarchically nanostructured electrodes, it is believed that the present hierarchical MoO_2 nanocrystal assemblies and ultrathin graphene sheets could

contribute to the enhanced electrochemical performances (*e.g.*, improved capacity and cyclability). It is also interesting to note that the capacity increases gradually over cycling, which has been often observed in the MoO_x-based electrode materials. Furthermore, the Ex-XRD patterns of the MoO_2/graphene electrodes after different discharge and charge cycles were obtained to investigate the structure evolution (Figure S13, see Supporting Information). After 70 discharge and charge cycles, the intensity of the XRD diffraction peaks of MoO_2 degrades. Meanwhile, there appear some new XRD peaks that cannot be assigned to the substance of Mo_xO_y or Mo. The gradually increased capacity over cycling may result from the improved Li-diffusion kinetics by an activation process associated with partial crystallinity degradation of the electrode to a disordered or amorphous-like structure during cycling.[28] The similar phenomenon is also observed in the other previous graphene-based hybrids.[23]

CONCLUSIONS

We have successfully demonstrated the large-scale fabrication of self-assembled MoO_2/graphene hierarchical nanoarchitectures for the first time. Results show that the as-formed hierarchical MoO_2/graphene hybrid exhibits highly reversible capacity, excellent cyclability, and high Coulombic efficiency with good rate capability as an anode material in lithium-ion batteries. This work provides a facile strategy to prepare hierarchically nanostructured MoO_2/graphene hybrids without using any seed crystals, templates, or organic additives, and therefore it is promising for large-scale industrial production. It is expected that the high-performance MoO_2/graphene hybrids may give rise to the substitution of conventional graphite for next-generation energy transfer and storage devices.

METHODS

Preparation of Graphene Oxide (GO). GO was prepared using a modified Hummers method.[41,42] In a typical procedure, 1 g of graphite and 0.75 g of $NaNO_3$ were placed in a flask. Then, 75 mL of H_2SO_4 (98 wt %) was added under stirring in an ice–water bath, and 4.5 g of $KMnO_4$ was slowly added over about 1 h. The mixture was continuously stirred for 2 h in the ice water bath. After the mixture was stirred vigorously for 5 days at room temperature, 3 mL of H_2O_2 (30 wt %) was added, and the mixture was continuously stirred for 2 h. Then, the GO product was collected and washed thoroughly using a mixed solution of 3 wt % H_2SO_4 and 0.5 wt % H_2O_2. Subsequently, the GO product was washed by deionized (DI) water until pH = 4, and then dispersed in DI water (10 mg mL^{-1}) under ultrasonication for 5 h to yield a homogeneous suspension.

Preparation of the MoO_2/Graphene Hybrid. An aqueous exfoliated GO suspension (100 mL, approximately 3 mg mL^{-1}), phosphomolybdic acid ($H_3PMo_{12}O_{40}\cdot xH_2O$) solution (100 mL, 15 mM), and DI water (100 mL) were mixed and sonicated at 30–40 °C for 30 min. Hydrazine hydrate (1.25 mL, 80 wt %) was then added under stirring. The mixture was sonicated for 3 h and kept at room temperature for another 3 h. The black solid was collected by filtration, and then washed with DI water and absolute ethanol for six times. The as-formed precursor was dried in vacuum at 80 °C and subsequently treated at 500 °C (ramp rate: 1 °C min^{-1}) in a 5% H_2/Ar atmosphere for 5 h. Finally, the black-colored product of the MoO_2/graphene hybrid was obtained. For comparison, the free MoO_2 particles were also prepared under the same condition instead of the addition of GO.

Materials Characterization. Power XRD patterns were collected using a X'Pert PRO (PANalytical B.V., Holland) diffractometer with high-intensity Cu Kα1 irradiation (λ = 1.5406 Å). The accelerating voltage and the applied current were 40 kV and 40 mA, respectively. The general morphology of the products was characterized by a FESEM (FEI, Sirion 200) coupled with an EDX (Oxford Instrument) spectrometer. TEM observations were carried out on a JEOL 2100F microscope. TG/DTA analyses were performed with a PerkinElmer Diamond TG/DTA apparatus at a heating rate of 10 °C min^{-1} in flowing air. XPS measurements were performed on a VG MultiLab 2000 system with a monochromatic Al Ka X-ray source (ThermoVG Scientific). Raman spectra were measured by using a Renishaw Invia spectrometer using Ar^+ laser of 514.5 nm at room temperature. The Brunauer–Emmett–Teller (BET) surface area and porosity were determined by nitrogen-sorption using a Micrometritics ASAP 2020 analyzer.

Electrochemical Measurements. The working electrodes were prepared by mixing 80 wt % active material (MoO_2/graphene hybrid, MoO_2 particles), 10 wt % acetylene black (Super-P), and 10 wt % polyvinylidene fluoride (PVDF) in *N*-methyl-2-pyrrolidinone. After coating the above slurries on Cu foils, the electrodes were dried at 80 °C in vacuum for 6 h to remove the solvent before pressing. Then the electrodes were cut into disks (8 mm in diameter) and dried at 80 °C for 24 h in vacuum. The coin cells were laboratory-assembled by a CR2032 press in an argon-filled glovebox where the moisture and oxygen concentrations were strictly limited to below 1 ppm. A lithium foil was used as the counter electrode, and a Celgard 2300 membrane was used as the separator. The commercial electrolyte was composed of 1 mol L^{-1} $LiPF_6$ in a mixture of ethylene carbonate (EC) and dimethyl carbonate (DMC) (*v*/*v* = 1:1). CV curves were recorded on a PARSTAT 2273 potentiostat at a scanning rate of 0.1 mV s^{-1} at room temperature. The galvanostatic charge–discharge tests were carried out on a Land Battery Measurement System (Land, China) at various current densities of 500–2000 mA g^{-1} with a cutoff voltage of 3.00–0.01 V *vs* Li/Li^+ at room temperature.

Acknowledgment. This work was supported by the Natural Science Foundation of China (Grant Nos. 50825203 and 51002057), the 863 program (Grant No. 2009AA03Z225), the Natural Science Foundation of Hubei Province (Grant No. 2008CDA026), the Fundamental Research Funds for the Central Universities (HUST: 2010QN007), and the PCSIRT (Program for Changjiang Scholars and Innovative Research Team in University). The authors thank Analytical and Testing Center of HUST for SEM measurements.

Supporting Information Available: Supplementary XRD, SEM, EDX, Raman spectrum, and additional electrochemical performance figures. This material is available free of charge *via* the Internet at http://pubs.acs.org.

REFERENCES AND NOTES

1. Nam, K. T.; Kim, D. W.; Yoo, P. J.; Chiang, C. Y.; Meethong, N.; Hammond, P. T.; Chiang, Y. M.; Belcher, A. M. Virus-Enabled Synthesis and Assembly of Nanowires for Lithium Ion Battery Electrodes. *Science* **2006**, *312*, 885–888.
2. Chan, C. K.; Peng, H.; Liu, G.; McIlwrath, K.; Zhang, X. F.; Huggins, R. A.; Cui, Y. High-Performance Lithium Battery Anodes Using Silicon Nanowires. *Nat. Nanotechnol.* **2008**, *3*, 31–35.

3. Kang, K.; Meng, Y. S.; Breger, J.; Grey, C. P.; Ceder, G. Electrodes with High Power and High Capacity for Rechargeable Lithium Batteries. *Science* **2006**, *311*, 977–980.
4. Li, H.; Wang, Z.; Chen, L.; Huang, X. Research on Advanced Materials for Li-Ion Batteries. *Adv. Mater.* **2009**, *21*, 4593–4607.
5. Yuan, L. X.; Wang, Z. H.; Zhang, W. X.; Hu, X. L.; Chen, J. T.; Huang, Y. H.; Goodenough, J. B. Development and Challenges of $LiFePO_4$ Cathode Material for Lithium-Ion Batteries. *Energy Environ. Sci.* **2011**, *4*, 269–284.
6. Chen, J.; Xu, L.; Li, W.; Gou, X. α-Fe_2O_3 Nanotubes in Gas Sensor and Lithium-Ion Battery Applications. *Adv. Mater.* **2005**, *17*, 582–586.
7. Ban, C.; Wu, Z.; Gillaspie, D. T.; Chen, L.; Yan, Y.; Blackburn, J. L.; Dillon, A. C. Nanostructured Fe_3O_4/SWNT Electrode: Binder-free and High-Rate Li-Ion Anode. *Adv. Mater.* **2010**, *22*, E145–E149.
8. Cao, A. M.; Hu, J. S.; Liang, H. P.; Wan, L. J. Self-Assembled Vanadium Pentoxide (V_2O_5) Hollow Microspheres from Nanorods and Their Application in Lithium-Ion Batteries. *Angew. Chem., Int. Ed.* **2005**, *44*, 4391–4395.
9. Shim, H. W.; Jin, Y. H.; Seo, S. D.; Lee, S. H.; Kim, D. W. Highly Reversible Lithium Storage in Bacillus Subtilis-Directed Porous Co_3O_4 Nanostructures. *ACS Nano* **2010**, *5*, 443–449.
10. Cabana, J.; Monconduit, L.; Larcher, D.; Palacín, M. R. Beyond Intercalation-Based Li-Ion Batteries: The State of the Art and Challenges of Electrode Materials Reacting Through Conversion Reactions. *Adv. Mater.* **2010**, *22*, E170–E192.
11. Bruce, P. G.; Scrosati, B.; Tarascon, J. M. Nanomaterials for Rechargeable Lithium Batteries. *Angew. Chem., Int. Ed.* **2008**, *47*, 2930–2946.
12. Magasinski, A.; Dixon, P.; Hertzberg, B.; Kvit, A.; Ayala, J.; Yushin, G. High-Performance Lithium-Ion Anodes Using a Hierarchical Bottom-Up Approach. *Nat. Mater.* **2010**, *9*, 353–358.
13. Mai, L.; Xu, L.; Han, C.; Xu, X.; Luo, Y.; Zhao, S.; Zhao, Y. Electrospun Ultralong Hierarchical Vanadium Oxide Nanowires with High Performance for Lithium Ion Batteries. *Nano Lett.* **2010**, *10*, 4750–4755.
14. Chen, J. S.; Tan, Y. L.; Li, C. M.; Cheah, Y. L.; Luan, D.; Madhavi, S.; Boey, F. Y. C.; Archer, L. A.; Lou, X. W. Constructing Hierarchical Spheres from Large Ultrathin Anatase TiO_2 Nanosheets with Nearly 100% Exposed (001) Facets for Fast Reversible Lithium Storage. *J. Am. Chem. Soc.* **2010**, *132*, 6124–6130.
15. Hu, Y. S.; Adelhelm, P.; Smarsly, B. M.; Hore, S.; Antonietti, M.; Maier, J. Synthesis of Hierarchically Porous Carbon Monoliths with Highly Ordered Microstructure and Their Application in Rechargeable Lithium Batteries with High-Rate Capability. *Adv. Funct. Mater.* **2007**, *17*, 1873–1878.
16. Sun, F.; Yu, J. C.; Wang, X. Construction of Size-Controllable Hierarchical Nanoporous TiO_2 Ring Arrays and Their Modifications. *Chem. Mater.* **2006**, *18*, 3774–3779.
17. Ariga, K.; Hill, J. P.; Lee, M. V.; Vinu, A.; Charvet, R.; Acharya, S. Challenges and Breakthroughs in Recent Research on Self-Assembly. *Sci. Adv. Mater.* **2008**, *9*, 014109.
18. Zhang, D. F.; Sun, L. D.; Jia, C. J.; Yan, Z. G.; You, L. P.; Yan, C. H. Hierarchical Assembly of SnO_2 Nanorod Arrays on α-Fe_2O_3 Nanotubes: A Case of Interfacial Lattice Compatibility. *J. Am. Chem. Soc.* **2005**, *127*, 13492–13493.
19. Zhang, W. M.; Wu, X. L.; Hu, J. S.; Guo, Y. G.; Wan, L. J. Carbon Coated Fe_3O_4 Nanospindles as a Superior Anode Material for Lithium-Ion Batteries. *Adv. Funct. Mater.* **2008**, *18*, 3941–3946.
20. Cui, G.; Hu, Y. S.; Zhi, L.; Wu, D.; Lieberwirth, I.; Maier, J.; Müllen, K. A. One-Step Approach Towards Carbon-Encapsulated Hollow Tin Nanoparticles and Their Application in Lithium Batteries. *Small* **2007**, *3*, 2066–2069.
21. Wang, X.; Zhou, X.; Yao, K.; Zhang, J.; Liu, Z. A SnO_2/Graphene Composite as a High Stability Electrode for Lithium Ion Batteries. *Carbon* **2011**, *49*, 133–139.
22. Zhou, G.; Wang, D. W.; Li, F.; Zhang, L.; Li, N.; Wu, Z. S.; Wen, L.; Lu, G. Q.; Cheng, H.-M. Graphene–Wrapped Fe_3O_4 Anode Material with Improved Reversible Capacity and Cyclic Stability for Lithium Ion Batteries. *Chem. Mater.* **2010**, *22*, 5306–5313.
23. Wu, Z. S.; Ren, W.; Wen, L.; Gao, L.; Zhao, J.; Chen, Z.; Zhou, G.; Li, F.; Cheng, H. M. Graphene Anchored with Co_3O_4 Nanoparticles as Anode of Lithium Ion Batteries with Enhanced Reversible Capacity and Cyclic Performance. *ACS Nano* **2010**, *4*, 3187–3194.
24. Wang, H.; Cui, L. F.; Yang, Y.; Casalongue, H. S.; Robinson, J. T.; Liang, Y.; Cui, Y.; Dai, H. Mn_3O_4–Graphene Hybrid as a High-Capacity Anode Material for Lithium Ion Batteries. *J. Am. Chem. Soc.* **2010**, *132*, 13978–13980.
25. Wang, D.; Choi, D.; Li, J.; Yang, Z.; Nie, Z.; Kou, R.; Hu, D.; Wang, C.; Saraf, L. V.; Zhang, J.; *et al.* Self-Assembled TiO_2–Graphene Hybrid Nanostructures for Enhanced Li-Ion Insertion. *ACS Nano* **2009**, *3*, 907–914.
26. Li, N.; Liu, G.; Zhen, C.; Li, F.; Zhang, L.; Cheng, H. M. Battery Performance and Photocatalytic Activity of Mesoporous Anatase TiO_2 Nanospheres/Graphene Composites by Template-Free Self-Assembly. *Adv. Funct. Mater.* **2011**, *21*, 1717–1722.
27. Murphy, D. W.; Salvo, F. J. D.; Carides, J. N.; Waszczak, J. V. Topochemical Reactions of Rutile Related Structures with Lithium. *Mater. Res. Bull.* **1978**, *13*, 1395–1402.
28. Shi, Y. F.; Guo, B. K.; Corr, S. A.; Shi, Q. H.; Hu, Y. S.; Heier, K. R.; Chen, L. Q.; Seshadri, R.; Stucky, G. D. Ordered Mesoporous Metallic MoO_2 Materials with Highly Reversible Lithium Storage Capacity. *Nano Lett.* **2009**, *9*, 4215–4220.
29. Koziej, D.; Rossell, M. D.; Ludi, B.; Hintennach, A.; Novák, P.; Grunwaldt, J. D.; Niederberger, M. Interplay between Size and Crystal Structure of Molybdenum Dioxide Nanoparticles—Synthesis, Growth Mechanism, and Electrochemical Performance. *Small* **2011**, *7*, 377–387.
30. Ji, X.; Herle, P. S.; Rho, Y.; Nazar, L. F. Carbon/MoO_2 Composite Based on Porous Semigraphitized Nanorod Assemblies from *in Situ* Reaction of Tri-block Polymers. *Chem. Mater.* **2007**, *19*, 374–383.
31. Ku, J. H.; Jung, Y. S.; Lee, K. T.; Kim, C. H.; Oh, S. M. Thermoelectrochemically Activated MoO_2 Powder Electrode for Lithium Secondary Batteries. *J. Electrochem. Soc.* **2009**, *156*, A688–A693.
32. Wang, Z.; Chen, J. S.; Zhu, T.; Madhavi, S.; Lou, X. W. One-Pot Synthesis of Uniform Carbon-Coated MoO_2 Nanospheres for High-Rate Reversible Lithium Storage. *Chem. Commun.* **2010**, *46*, 6906–6908.
33. Gao, Q. S.; Yang, L. C.; Lu, X. C.; Mao, J. J.; Zhang, Y. H.; Wu, Y. P.; Tang, Y. Synthesis, Characterization and Lithium-Storage Performance of MoO_2/Carbon Hybrid Nanowires. *J. Mater. Chem.* **2010**, *20*, 2807–2812.
34. Park, C. M.; Kim, J. H.; Kim, H.; Sohn, H. J. Li-Alloy Based Anode Materials for Li Secondary Batteries. *Chem. Soc. Rev.* **2010**, *39*, 3115–3141.
35. Moulder, J. F.; Stickle, W. F.; Sobol, P. E.; Bomben, K. D. *Handbook of X-ray Photoelectron Spectroscopy*; Chastain, J., Ed.; Perkin-Elmer Corporation: Eden Prairie, MN, 1992.
36. Yang, L. C.; Gao, Q. S.; Tang, Y.; Wu, Y. P.; Holze, R. MoO_2 Synthesized by Reduction of MoO_3 with Ethanol Vapor as an Anode Material with Good Rate Capability for the Lithium Ion Battery. *J. Power Sources* **2008**, *179*, 357–360.
37. Stankovich, S.; Piner, R. D.; Chen, X.; Wu, N.; Nguyen, S. T.; Ruoff, R. S. Stable Aqueous Dispersions of Graphitic Nanoplatelets *via* the Reduction of Exfoliated Graphite Oxide in the Presence of Poly(sodium 4-styrenesulfonate). *J. Mater. Chem.* **2006**, *16*, 155–158.
38. Schniepp, H. C.; Li, J. L.; McAllister, M. J.; Sai, H.; HerreraA-lonso, M.; Adamson, D. H.; Prud'homme, R. K.; Car, R.; Saville, D. A.; Aksay, I. A. Functionalized Single Graphene Sheets Derived from Splitting Graphite Oxide. *J. Phys. Chem. B* **2006**, *110*, 8535–8539.
39. Tuinstra, F.; Koenig, J. L. Raman Spectrum of Graphite. *J. Chem. Phys.* **1970**, *53*, 1126–1130.
40. Dahn, J. R.; McKinnon, W. R. Structure and Electrochemistry of Li_xMoO_2. *Solid State Ionics* **1987**, *23*, 1–7.
41. Hummers, W. S.; Offeman, R. E. Preparation of Graphitic Oxide. *J. Am. Chem. Soc.* **1958**, *80*, 1339–1339.
42. Hontoria-Lucas, C.; López-Peinado, A. J.; López-González, J.; De, D.; Rojas-Cervantes, M. L.; Martín-Aranda, R. M. Study of Oxygen-Containing Groups in a Series of Graphite Oxides: Physical and Chemical Characterization. *Carbon* **1995**, *33*, 1585.